Journal of Advanced Research 17 (2019) 55–63

Contents lists available at ScienceDirect

Journal of Advanced Research

journal homepage: www.elsevier.com/locate/jare

Original article

Magnetic activated carbon nanocomposite from *Nigella sativa* L. waste (MNSA) for the removal of Coomassie brilliant blue dye from aqueous solution: Statistical design of experiments for optimization of the adsorption conditions

Nour T. Abdel-Ghani [a], Ghadir A. El-Chaghaby [b,*], El-Shaimaa A. Rawash [b], Eder C. Lima [c]

[a] *Chemistry Department, Faculty of Science, Cairo University, Giza 12613, Egypt*
[b] *RCFF, Agricultural Research Center, 588 El-Orman, Giza, Egypt*
[c] *Institute of Chemistry, Federal University of Rio Grande do Sul (UFRGS), Av. Bento Gonçalves, 9500, 91501-970, P.O. Box 15003, Porto Alegre, RS, Brazil*

HIGHLIGHTS

- The successful preparation of novel magnetized activated carbon using *Nigella sativa* waste was achieved.
- The removal of Coomassie brilliant blue dye from aqueous solution by the prepared adsorbent was performed.
- Four factors affecting the adsorption process of Coomassie dye by the magnetized carbon were studied.
- The adsorption process was optimized using a factorial design of experiments with central points.
- The desirability was assessed for the two different studied responses, removal percentage and adsorption capacity.

GRAPHICAL ABSTRACT

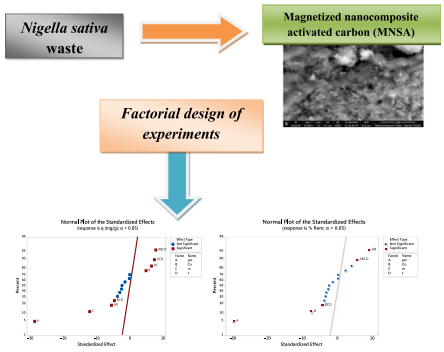

ARTICLE INFO

Article history:
Received 13 October 2018
Revised 16 December 2018
Accepted 17 December 2018
Available online 18 December 2018

Keywords:
Nigella sativa L. waste
Nanocomposite
Coomassie brilliant blue
Central composite design
Adsorption

ABSTRACT

The present work was carried out to evaluate the removal of Coomassie brilliant blue dye by adsorption onto a magnetized activated carbon nanocomposite (MNSA) prepared from *Nigella sativa* L. (NS) waste. Different techniques, including infrared spectroscopy, scanning electron microscopy, and nitrogen adsorption/desorption, were used to characterize MNSA to investigate its adsorption properties. Adsorption experiments were carried out by simultaneously optimizing four variables that usually present a strong effect in adsorption studies. A full 2^4 factorial design with 3 central points was used. The four independent variables were the initial pH of the dye solution (pH), the initial dye concentration (C_o), the adsorbent mass (m), and the contact time (t). The sorption capacity (q) of the adsorbent and the percentage of dye removal (% Rem) from an aqueous solution were used as the responses of the factorial design. The results indicated that pH, C_o, and m were essential factors for the overall optimization of both responses (q and % Rem) and that several interactions of two, three and four factors occurred. Based on the design of the experiments (DOE), the optimized conditions for adsorption were pH = 2.00, C_o = 40.0 mg L^{-1}, m = 30.0 mg, and t = 3.0 h. Under these conditions, both responses, q and % Rem, were maximized, with a desirability of 85.54%. The findings of this study could be useful for industrial wastewater treatment systems.

Peer review under responsibility of Cairo University.
* Corresponding author.
E-mail address: ghadiraly@yahoo.com (G.A. El-Chaghaby).

https://doi.org/10.1016/j.jare.2018.12.004
2090-1232/

Introduction

Coomassie brilliant blue dye is a synthetic dye commonly used in the textile industry and represents a toxic and unmanageable organic pollutant [1]. This dye has several industrial applications due to its intense colour and simplicity of application. Effluents containing Coomassie dye have several adverse effects on the eco-aquatic system [2]. Water-soluble dyes are poorly biodegradable, and according to Sandhya et al. [3], 20–50% of the overall dye remains in effluents as a result of the manufacturing process. As legislation has become more stringent, considerable importance has been given to the treatment of dye-containing effluents [4]. Therefore, it is highly desirable to remove dyes in general and Coomassie brilliant blue in particular from wastewater. Since synthetic dyes are inherently prepared as stable and non-degradable molecules, conventional treatment methods are not suitable for removal of such dyes from the aqueous phase. Over the years, the possibility of techniques such as oxidative degradation, electrocoagulation, membrane-based separation and biochemical degradation have been exploited, but these methods have drawbacks due to their inapplicability to large-scale units along with their energy- and chemical-intensive nature [5].

Nevertheless, adsorption is an effective method for dye removal from the aqueous phase because of its simple operation, low initial cost of implementation, high tolerance to concomitant species, ability to treat concentrated wastewater contaminated with different dyes and the possibility of reusing the spent adsorbent via regeneration. Subsequently, a variety of activated carbon-based adsorbents derived from various materials have been investigated for their efficacy and efficiency in the removal of dyes. However, the large volume of wastewater with high dye concentrations has inspired the development of non-toxic, low-cost and efficient adsorbents with the possibility of regeneration for reuse. Unfortunately, activated carbons are difficult to isolate from solution and are discarded with processed sludge after use in water and wastewater treatment, causing secondary pollution [6]. Among several studied adsorbents, magnetized adsorbents have shown high efficiency for the removal of dyes from effluents owing to their easy control and fast separation by direct application of a magnetic field [7–14]. The high adsorption capacity of magnetized adsorbents for dyes has been ascribed to the interactions of hydroxyl groups with the dye molecules [5]. In adsorption-based methods, it is desirable to know the process variables and their influence on the adsorption capacity to increase the contaminant removal efficiency of the adsorbent. The liquid-solid interface adsorption process is mainly affected by the initial concentration of the adsorbate, initial pH of the solution, adsorbent dose, surface area of the adsorbent, contact time, and temperature [15–17].

Optimization of the process variables is required to achieve the maximum adsorption capacity and removal efficiency of the adsorbent. The conventional method for the optimization of process variables requires a vast number of experiments to be performed, which increases costs and is time consuming. Additionally, the conventional approach does not verify the effects of interactions between the process variables on the dependent variables. The design of experiments (DOE) approach is a successful process for planning experimental runs. DOE generates an optimum experimental plan, decreasing the amount of chemicals used and the experimental time, thus leading to a better performance of experiments using less time [18]. The specific aims of the present study were to develop a novel magnetized activated carbon prepared from *Nigella sativa* L. waste and to apply a full factorial design with central points to obtain the maximum adsorption capacity of the developed magnetic nanocomposite for Coomassie brilliant blue dye removal from aqueous solution. This study consisted of examining the effects of four independent variables (initial dye concentration, initial pH of the dye solution, adsorbent dose, and contact time) and their interactions on the adsorption capacity of the magnetized carbon for Coomassie brilliant blue dye.

Material and methods

Preparation of the adsorbent

Magnetized carbon-iron oxide composite was prepared using carbon from *Nigella sativa* waste (NSW), an agro-waste material. NSW was obtained from a local factory in Egypt and treated with n-hexane followed by deionized water (DW) before oven drying at 100 °C to constant weight. The resulting material was then carbonized at 600 °C. The magnetized carbon-iron oxide composite derived from NSW was prepared following the procedure of Gupta and Nayak [19] with little modification. In 100 mL DW, ferric chloride (6.1 g) (Merck, Darmstadt, Germany) and ferrous sulfate (4.2 g) (Merck, Darmstadt, Germany) were dissolved and heated to 90 °C. Then, 10 mL of sodium hydroxide (2 M) (Merck, Darmstadt, Germany) and a solution of 1.00 g of NS carbon suspended in 200 mL of DW were quickly and consecutively added. The mixture was stirred for 30 min at 80 °C and then allowed to sitto reach room temperature. The black precipitate was filtered, washed and dried at 50 °C.

Characterization of the prepared adsorbent

The surface texture of the adsorbent was investigated using a JSM-6390LV instrument (JEOL Ltd, Tokyo, Japan) with a 3 kV accelerating voltage after drying the sample overnight at approximately 105 °C under vacuum before scanning electron microscopy (SEM) analysis. The surface functional groups on *N. Sativa* carbon and its magnetized carbon were studied using a Fourier transform infrared (FTIR) spectrophotometer (AVATAR 370 Csl, Thermo Nicolet Co., Massachusetts, USA) at a resolution of 4 cm^{-1} over the range of 500–4000 cm^{-1}. The samples were examined as KBr pellets (Thermo Fisher Scientific, Geel, Belgium). The textural properties of surface areas (S_{BET}) were determined from the Brunauer-Emmett-Teller (BET) method. The Barrett-Joyner-Halenda (BJH) method was used to calculate pore size. The textural characterization of the carbon material was obtained using nitrogen adsorption/desorption isotherms (Micromeritics Instrument Co., model TriStar II 3020- Atlanta, Georgia, USA). The surface area analyser was operated at −196 °C after drying the solid sample for 8 h at 150 °C at a pressure of < 2 mbar. The magnetic properties of magnetized *Nigella sativa* L. Activated carbon (MNSA) were confirmed using a Lake Shore7400 vibrating sample magnetometer (VSM) (California, USA).

Preparation of dye solutions

Stock solutions of the dye were prepared by dissolving the desired amount of Coomassie brilliant blue (C.I. 42660, Sigma-Aldrich, Switzerland) in DW. The pH of the test solution was adjusted using reagent-grade diluted hydrochloric acid.

Process variables and experimental design

Four variables (initial dye concentration (C_o), initial pH of the dye solution (pH), mass of adsorbent (m), and contact time(t)) were identified to investigate their influence on the adsorption capacity of MNSA for Coomassie brilliant blue dye (C.I. 42660). A full factorial 2^4 design with 3 central points (total of 19 experiments) was adopted to verify the effect of the described variables on the percentage of dye removal (% Rem) and the adsorption

capacity of the adsorbent (q). The selected variables with their values are given in Table 1.

It was hypothesized that the four independent variables and the experimental response data follow a linear equation, given in Eq. (1) [20]:

$$R = \beta 0 + \beta 1X1 + \beta 2X2 + \beta 3X3 + \beta 4X4 + \beta 5X1X2 + \beta 6X1X3 + \beta 7X1X4 + \beta 8X2X3 + \beta 9X2X4 + \beta 10X3X4 + \beta 11X1X2X3 + \beta 12X1X2X4 + \beta 13X1X3X4 + \beta 14X2X3X4 + \beta 15X1X2X3X4 + \varepsilon \quad (1)$$

where R is the predicted response (% Rem or q); X_1 to X_4 are the coded variables; β_o is the constant coefficient; β_1 to $\beta 4$ are the linear term coefficients; β_5 to β_{10} are the interaction coefficients between two variables; β_{11} to β_{14} are the interaction coefficients among three variables; β_{15} is the interaction coefficient among four variables; and ε is the experimental error [20].

Batch adsorption design

Batch experiments based on a 2^4 full factorial design plus 3 central points were conducted randomly to investigate the effect of the four pre-selected operating variables on q and % Rem with MNSA. For adsorption of the dye on the developed magnetic adsorbent, different amounts of adsorbent (30.0–50.0 mg) were added to 50.00 mL of solution initially containing 40.00 to 80.00 mg L^{-1} of the dye. Standard solutions of the dye were prepared by diluting the stock solution, and the pH was adjusted to 2.00–4.00 by using diluted hydrochloric acid. The adsorption experiments were conducted in a thermo-controlled (±1 °C) (Oxylab, São Leopoldo, Brazil) water bath shaker for different time intervals (1.00 to 3.00 h) at 50 rpm. The ranges of the initial pH of the solution were chosen according to previous experiments. Samples were removed and centrifuged after reaching equilibrium. The remaining concentration of dye in the solution was then determined using a visible spectrophotometer at a λ_{max} of 551 nm (UV-1280 Shimadzu, Kyoto, Japan).

The adsorbed quantity expressed per unit mass of magnetic activated carbon and the percentages of dye removal are given by Eqs. (2) and (3), respectively:

$$q = V.\frac{(C_0 - C_f)}{m} \quad (2)$$

$$\%Rem = 100.\frac{C_0 - C_f}{C_i} \quad (3)$$

where q is the amount of dye adsorbed by the adsorbent (mg g^{-1}); C_o is the initial dye concentration in contact with the adsorbent (mg L^{-1}); C_f is the dye concentration after the batch adsorption study (mg L^{-1}); m is the mass of adsorbent (g); and V is the volume of the dye solution (L).

Results and discussion

FTIR spectral analysis of adsorbent

Fig. 1(A, B) illustrates the FTIR spectra of (A) *N. sativa* carbon (NSC) and (B) MNSA. The spectra revealed a broad and strong band at approximately 3406 cm^{-1}, which is characteristic of the stretching vibration of O—H in the hydroxyl groups of hydrogen bonds [1]. The bands in the region between 1452 and 908 cm^{-1} could be assigned to C—O stretching vibrations [21]. The intense broadband positioned at1080 cm^{-1} in NSC, which was shifted to 1119 cm^{-1} in MNSA, could be attributed to C—O vibrations in secondary and primary R–OH groups in alcohols [1]. The small bands at 908, 717, and 611 cm^{-1} were attributed to the out-of-plane bending vibrations of C—H in benzene derivatives, and the medium-width intense band at 563 cm^{-1} is ascribed to O—H bending. The new peak at 591 cm^{-1} in the MNSA spectrum was assigned to Fe—O [22]. A comparison of the NSC and MNSA spectra indicated the disappearance, shifting, and emergence of individual peaks. Significant band

Table 1
Experiments performed for the 2^4 full factorial design with 3 central points. The responses of this factorial design were% Rem and q. Values of responses are given with four significant digits.

Exp.	pH	C_o (mg L^{-1})	Mass (mg)	Time (h)	% Rem	q (mg g^{-1})
1	2.00	40.00	30.0	1.00	81.18	54.12
2	4.00	40.00	30.0	1.00	9.760	6.520
3	2.00	80.00	30.0	1.00	30.20	40.20
4	4.00	80.00	30.0	1.00	20.77	27.68
5	2.00	40.00	50.0	1.00	60.00	24.00
6	4.00	40.00	50.0	1.00	3.560	1.420
7	2.00	80.00	50.0	1.00	62.60	50.00
8	4.00	80.00	50.0	1.00	9.800	7.800
9	2.00	40.00	30.0	3.00	85.88	57.25
10	4.00	40.00	30.0	3.00	5.580	3.710
11	2.00	80.00	30.0	3.00	58.70	78.25
12	4.00	80.00	30.0	3.00	1.240	1.680
13	2.00	40.00	50.0	3.00	76.47	30.59
14	4.00	40.00	50.0	3.00	0.000	0.000
15	2.00	80.00	50.0	3.00	30.69	24.55
16	4.00	80.00	50.0	3.00	0.000	0.000
17	3.00	60.00	40.0	2.00	25.03	18.77
18	3.00	60.00	40.0	2.00	19.30	14.50
19	3.00	60.00	40.0	2.00	26.10	19.50

		Levels of the variables		
	Variable	−1	0	1
pH	X_1	2.00	3.00	4.00
C_o (mg L^{-1})	X_2	40.00	60.00	80.00
Mass (mg)	X_3	30.00	40.00	50.00
Time (h)	X_4	1.00	2.00	3.00

The coded level −1 stands for the lowest value of the parameter, the +1 level stands for the highest value of the parameter, and 0 stands for the central point, that is, the median of the −1 and +1 values of each parameter.

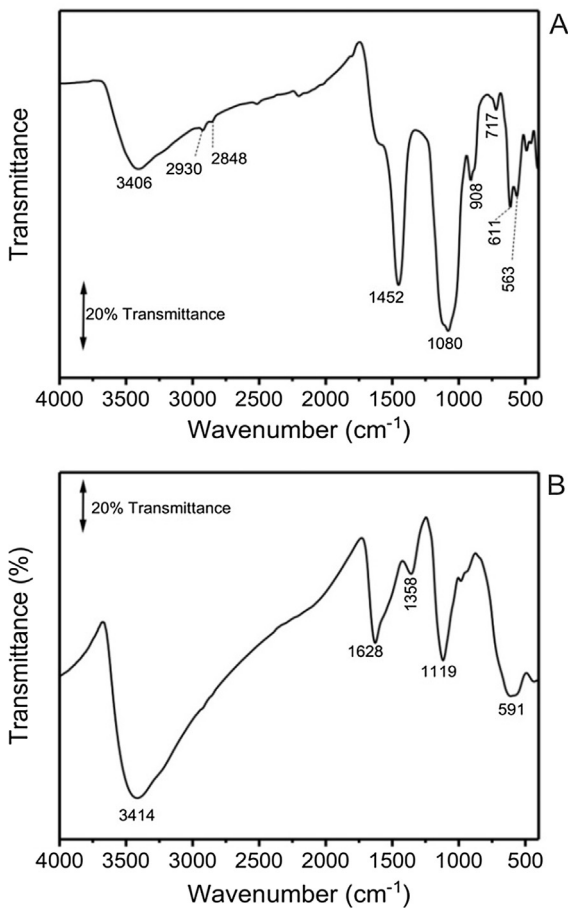

Fig. 1. FTIR spectra of (A) *N. sativa* carbon (NSC) and (B) magnetized *N. sativa* (MNSA).

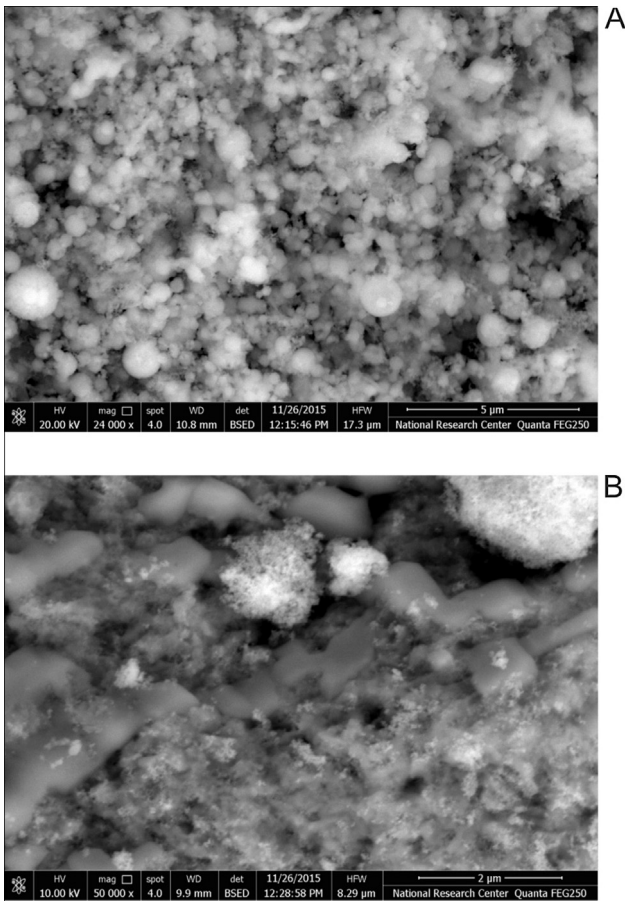

Fig. 2. Micrographs of (A) *N. sativa* carbon (NSC) and (B) magnetized *N. sativa* (MNSA) × 50,000.

shifts from 1452 cm^{-1} (O═C—OH carboxyl stretching) and 1080 cm^{-1} (C—O stretching) on NSC to 1358 cm^{-1} and 1119 cm^{-1}, respectively, on MNSA were also observed. In addition, a new peak appeared at 591 cm^{-1} in the MNSA spectrum, which was attributed to the formation of Fe—O. The peak shifts of the O═C—OH of carboxyl and C—O of alcohol in NSC relative to their locations in MNSA were due to the interactions of iron compounds with these groups. The analysis of the FTIR spectra indicated the formation of MNSA [19].

Scanning electron microscopy (SEM) analysis

SEM analysis was performed on both NSC and MNSA to study their surface porosity development. Fig. 2A shows an SEM micrograph of NSC, the surface of which had small pores; in contrast, the SEM micrograph of MNSA in Fig. 2B shows larger developed pores on the surface of MNSA, which enhanced the adsorption process and removal efficiency. This difference in pore size could be due to the contribution of iron oxide in the ash composite, which improved the surface morphology and surface properties of the material.

Textural characteristics of the adsorbent material

The surface area and total pore volume of the magnetic carbon material were 106.4 $m^2\ g^{-1}$ and 0.220 g cm^{-3}, respectively, which are compatible with the previously reported properties of magnetic composites comprising carbon materials loaded with magnetic iron compounds [23–26].

Magnetic properties of the adsorbent

The magnetic properties of MNSA were confirmed by hysteresis loops obtained from plots of magnetization against field strength, as shown in Fig. 3 [27].

Full factorial design

A factorial design is applied to minimize the total number of experimental runs to attain the optimization of a whole system

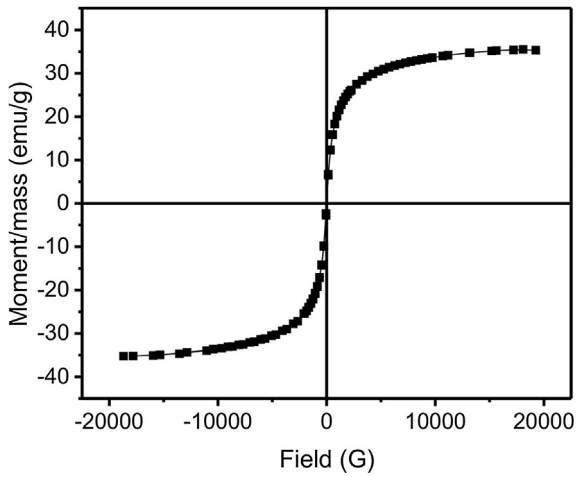

Fig. 3. Magnetic moment of magnetic and nonmagnetic activated carbons.

[11,15–17,28,29]. The design verifies the factors that have essential effects on a response and shows how the effect of a factor changes with the levels of other factors [30].

Dye adsorption by an adsorbent in a batch system typically depends on various factors, such as solution pH, adsorbate concentration, adsorbent mass, contact time, and temperature. The optimization of all these variables using a univariate procedure is tedious because each variable (factor) is optimized by varying just one specific factor and keeping the others constant. Then, the best value attained for that specific factor is fixed, and the other factors are varied in turn [31]. The drawback of this one-factor process is that the best conditions cannot be reached because the interactional effects of the factors are ignored; in addition, it is not possible to predict whether the same optimization would be attained if the levels of other variables were changed. Additionally, the total number of experiments to be performed in the univariate procedure is much higher than that when using a statistical DOE [31].

In this work, the factors monitored were pH (X_1), initial dye concentration (X_2), adsorbent mass (X_3) and contact time between MNSA and dye (X_4) to determine the maximum q and % Rem. The experiments in Table 1 (n = 19) were carried out to obtain the two responses of the system; q was expressed in milligrams of dye per gram of adsorbent, and % Rem was expressed as a percentage. The definitions of the factors and the levels used in the complete design are presented in Table 1. The main and interaction effects, model coefficients, standard deviations, and probabilities for the full 2^4 factorial design for the responses of q and % Rem are presented in Tables 2 and 3, respectively.

Table 2
Factorial Fit: q versus pH, C_o, m, t and central point.

Term	Effect	Coefficient	SE of coefficient	*P*
Constant		25.49 (β_0)	0.6750	0.001
Main factors				
pH (X_1)	−38.77	−19.38 (β_1)	0.6750	0.001
C_o (X_2)	6.569	3.285 (β_2)	0.6750	0.040
M (X_3)	−16.38	−8.191 (β_3)	0.6750	0.007
t (X_4)	−1.964	−0.9820 (β_4)	0.6750	0.283
2-way interaction				
pH·C_o (X_1X_2)	−0.1920	−0.09600 (β_5)	0.6750	0.900
pH·m (X_1X_3)	8.789	4.394 (β_6)	0.6750	0.023
pH·t (X_1X_4)	−7.544	−3.772 (β_7)	0.6750	0.031
C_o·m (X_2X_3)	$1.600.10^{-2}$	$8.000.10^{-3}$ (β_8)	0.6750	0.991
C_o·t (X_2X_4)	−3.336	−1.668 (β_9)	0.6750	0.132
m·t (X_3X_4)	−5.057	−2.528 (β_{10})	0.6750	0.064
3-way interaction				
pH·C_o·m ($X_1X_2X_3$)	−3.204	−1.602 (β_{11})	0.6750	0.141
pH·C_o·t ($X_1X_2X_4$)	−4.056	−2.028 (β_{12})	0.6750	0.095
pH·m·t ($X_1X_3X_4$)	9.954	4.977 (β_{13})	0.6750	0.018
C_o·m·t ($X_2X_3X_4$)	−6.268	−3.134 (β_{14})	0.6750	0.043
4-way interaction				
pH·C_o·m·t ($X_1X_2X_3X_4$)	10.47	5.235 (β_{15})	0.6750	0.016
Central point (cp)		−7.900	1.700	0.043
S = 2.701	R^2 = 0.9984	R^2_{adj} = 0.9858		

Estimated effects and coefficients for q (coded units). Full 2^4 factorial design. The effects and coefficients are given in coded units. All values are expressed with 4 significant digits, except probability (P), which is expressed with three decimal places.

Table 3
Analysis of variance factorial fit: q versus pH; Co, m, t, and central point.

Source	DF	Contribution	Adj. SS	Adj. MS	F-value	*P*-value
Model	16	99.84%	9213.30	575.83	78.94	0.013
Linear	4	78.82%	7273.34	1818.33	249.28	0.004
pH	1	65.15%	6011.91	6011.91	824.19	0.001
C_o	1	1.87%	172.62	172.62	23.67	0.040
m	1	11.63%	1073.38	1073.38	147.15	0.007
t	1	0.17%	15.43	15.43	2.11	0.283
2-way interaction	6	7.41%	683.55	113.93	15.62	0.061
pH.Co	1	0.00%	0.15	0.15	0.020	0.900
pH.m	1	3.35%	308.97	308.97	42.36	0.023
pH.t	1	2.47%	227.63	227.63	31.21	0.031
C_o.m	1	0.00%	0.00	0.00	0.00	0.991
C_o.t	1	0.48%	44.52	44.52	6.10	0.132
m.t	1	1.11%	102.28	102.28	14.02	0.064
3-way interaction	4	7.16%	660.38	165.10	22.63	0.043
pH.Co.m	1	0.44%	41.06	41.06	5.63	0.141
pH.Co.t	1	0.71%	65.81	65.81	9.02	0.095
pH.m.t	1	4.30%	396.35	396.35	54.34	0.018
C_o.m.t	1	1.70%	157.16	157.16	21.55	0.043
4-way interaction	1	4.75%	438.55	438.55	60.12	0.016
pH.Co.m.t	1	4.75%	438.55	438.55	60.12	0.016
Central point (cp)	1	1.71%	157.48	157.48	21.59	0.043
Error	2	0.16%	14.59	7.29		
Total	18	100.00%				

For the response q (Table 2), all the main factors were significant with a probability level $P \leq 0.05$, except (X_4). All the main effects and interactions that presented probabilities lower than 0.05 were significant (see Table 2). Regarding the interaction factors, two interactions of 2 factors, two interactions of 3 factors and one interaction of 4 factors were significant at the 5% significance level ($P \leq 0.05$). The fit model presented an adjusted squared determination coefficient (R^2_{adj}) of 0.9858, fitting the statistical model very well.

Thus, q could be expressed as Eq. (4):

$$q = 25.49 - 19.38pH + 3.285C_o - 8.191m + 4.394pH \cdot m - 3.772pH \cdot t + 4.977pH \cdot m \cdot t - 3.134\ C_o \cdot m \cdot t + 5.235pH \cdot C_o \cdot m \cdot t \quad (4)$$

In Eq. (4), the values of the factors are coded, and the levels are valid only in the intervals described in Table 1 (from −1 to + 1). The uncertainty of this equation is only 1.42%, based on the R^2_{adj}. Positive coefficients mean that an increase in the levels of the corresponding factor led to an increase in q; in contrast, negative coefficients led to a decrease in the response (q) when the corresponding levels were increased.

To better evaluate each factor and its interactions, Fig. 4A presents the normal probability plot of standardized effects. This graph is divided into two regions: the region where the factors and their interactions presented negative effects (pH, m, X·t, pH·t, C_o·m·t) and the region where the factors and interactions had positive effects (C_o, pH·m, pH·m·t, pH·C_o·m·t). All of these factors and

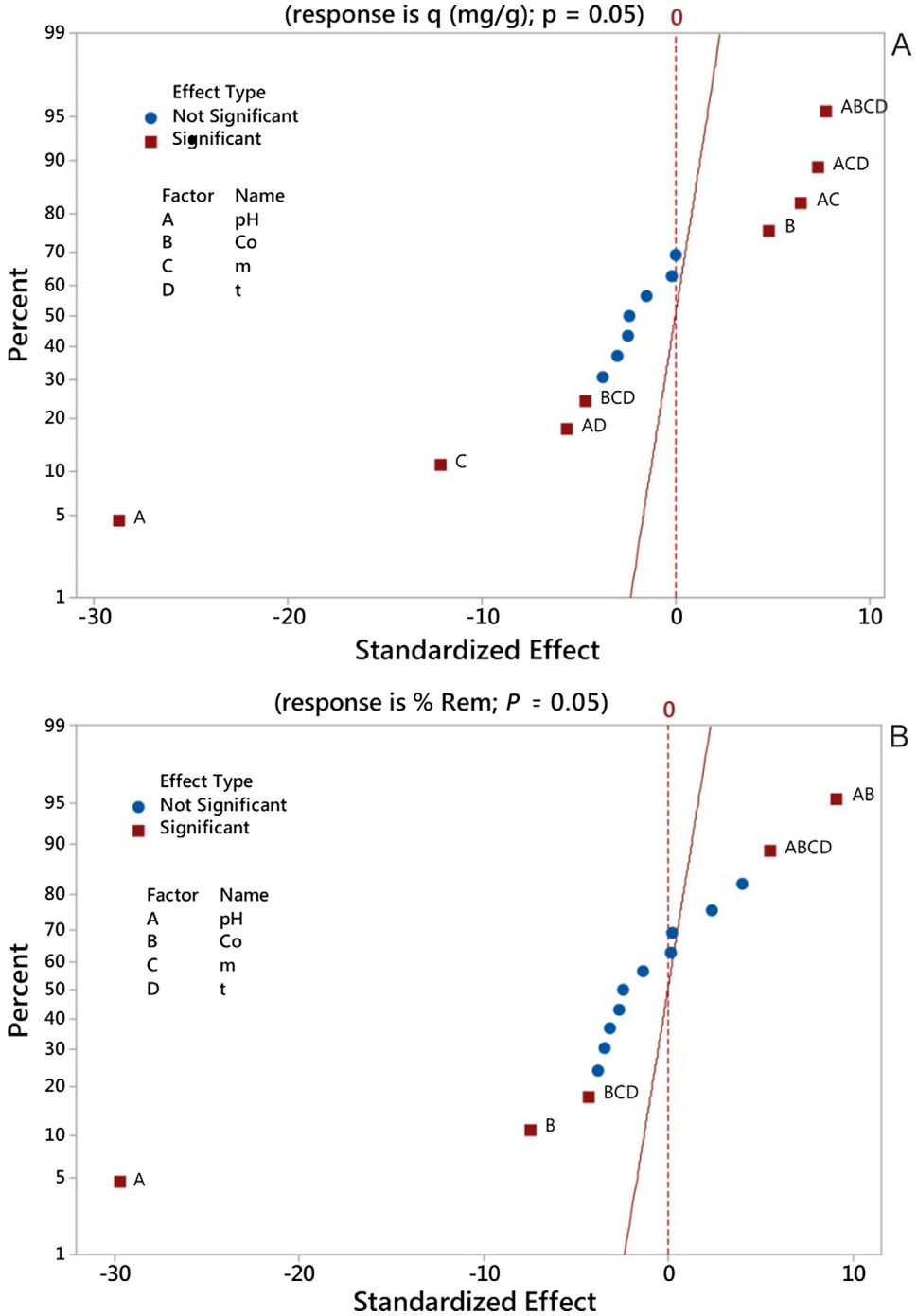

Fig. 4. Normal probability plot of standardized effects for (A) adsorption capacity (q) and (B) percent removal (% Rem).

interactions, which were represented as squares, were significant, and the terms fell outside the central line that crosses the zero value at the abscissa at a 50% probability. A circle represents the effects along this line, corresponding to the estimated errors of the effects, which were not significant ($p \geq 0.05$, see Table 2). The analysis of variance of the factorial fit of q versus pH, C_o, m, and t gave the contribution of each factor and its interaction as a percentage (see Table 3). Additionally, all factors and interactions with a probability ≤5% ($P \leq 0.05$) were significant at the 95% probability level.

By analysing the graph in Fig. 4A and the values in Table 2 and Table 3, it can be inferred that pH was the most critical variable in the overall adsorption procedure (65.15%). The negative coefficient of pH means that the adsorbance of the adsorbate by MNSA was favoured at low pH values (pH 2.0). An increase in pH led to a remarkable decrease in dye adsorption by the magnetic adsorbent. These results are in agreement with Royer et al. [32] and da Silva et al. [33]. For further optimization experiments, the pH was kept at 2.0 to prevent the leaching out of iron from the magnetic adsorbent at lower pH values [31].

The next most important factor for overall optimization of the batch system was m (11.63%). An increase in m led to a decrease in q, as expected [34]. This correlation occurred because an increase in mat a preset volume and concentration of dye leads to the non-saturation of adsorption sites as adsorption progresses; furthermore, the decrease in q may be due to particle aggregation resulting from the high m. Such aggregation would lead to a reduction in the total surface area of the adsorbent and an increase in the diffusional path length [34].

The third most important factor for overall optimization of the adsorption system was the interaction of four factors (pH·C_o·m·t) (4.75%), which was more significant than the main factor C_o (1.87%). This result rationalizes the benefits of using a factorial DOE rather than a conventional univariate process for adsorption method optimization [31] because this interactive relationship would not be identified in univariate optimization of a batch adsorption system. This interaction had appositive coefficient. The fourth most important factor for the overall optimization of the batch contact adsorption system was an interaction of three factors (pH·m·t) (4.30%), followed by the fifth most important factor, which was the interaction of two factors (pH·m) (3.35%); both factors had a positive coefficient. The sixth most important factor was the interaction of two factors (pH·t) (2.47%), with a negative coefficient. The seventh most important factor was C_o(1.87%), which had a positive coefficient and was followed by an interaction of three factors (C_o·m·t) (1.70%), which had a negative coefficient and was ranked eighth in relation to the overall optimization of the response (q).

For the response of % Rem (Table 4 and Table 5), the main factors that were significant at the 5% significance level ($P \leq 0.05$) were pH (75.83% overall response) and C_o(4.71%). Regarding the interaction factors, there was one interaction of 2 factors (pH·C_o) (7.22%), one interaction of three factors (C_o·m·t) (1.59%) and one interaction of four factors (pH·C_o·m·t) (2.65%).

The model had an R^2 of 0.9983, thus fitting the statistical model very well.

Estimated effects and coefficients for % Rem (coded units). Full 2^4 factorial design. The effects and coefficients are given in coded units. All values are expressed with 4 significant digits, except probability (*P*), which is expressed with three decimal places.

Thus, % Rem could be expressed as Eq. (5):

$$\%\ \text{Rem} = 33.53 - -27.19\text{pH} - 6.776C_o + 8.390\text{pH} \cdot C_o - 3.942C_o \cdot m \cdot t + 5.081\text{pH} \cdot C_o \cdot m \cdot t \quad (5)$$

In Eq. (5), the values of the factors are coded, and the levels correspond to the levels described in Table 1. The uncertainty of this equation is only 1.54%, based on R^2_{adj}.

Analysis of the graph in Fig. 4B and the values in Tables 4 and 5 shows that pH is the variable that presents the most relevant influence on the overall optimization of % Rem. Additionally, the negative coefficient of this variable indicates that an increase in pH would lead to a decrease in% Rem. As stated before, further experiments were carried out at pH 2.0. The second most important factor for optimization of the response was the interaction of pH·C_o, which was more relevant to the response than the main factor C_o. This information is beneficial for the optimization of the batch contact adsorption system and would not be obtained using univariate optimization. A small negative error in pH in conjunction with a small error in C_o would lead to an expected

Table 4
Factorial fit: % Rem versus pH, C_o, m, t and central point.

Term	Effect	Coefficient	SE of coefficient	*P*
Constant		33.53 (β_0)	0.9140	0.001
Main factors				
pH (X_1)	−54.38	−27.19 (β_1)	0.9140	0.001
C_o (X_2)	−13.553	−6.776 (β_2)	0.9140	0.018
m (X_3)	−6.273	−3.136 (β_3)	0.9140	0.075
t (X_4)	−2.414	−1.207 (β_4)	0.9140	0.318
2-way interaction				
pH·C_o (X_1X_2)	16.78	8.390 (β_5)	0.9140	0.012
pH·m (X_1X_3)	0.2750	0.1380 (β_6)	0.9140	0.894
pH·t (X_1X_4)	−6.854	−3.427 (β_7)	0.9140	0.064
C_o·m (X_2X_3)	4.318	2.159 (β_8)	0.9140	0.142
C_o·t (X_2X_4)	−5.771	−2.886 (β_9)	0.9140	0.087
m·t (X_3X_4)	−4.786	−2.393 (β_{10})	0.9140	0.120
3-way interaction				
pH·C_o·m ($X_1X_2X_3$)	−4.425	−2.213 (β_{11})	0.9140	0.137
pH·C_o·t ($X_1X_2X_4$)	0.3740	0.1870 (β_{12})	0.9140	0.857
pH·m·t ($X_1X_3X_4$)	7.374	3.687 (β_{13})	0.9140	0.056
C_o·m·t ($X_2X_3X_4$)	−7.884	−3.942 (β_{14})	0.9140	0.050
4-way interaction				
pH·C_o·m·t ($X_1X_2X_3X_4$)	10.16	5.081 (β_{15})	0.9140	0.031
Central point (cp)		−10.05	2.300	0.049
S = 3.656	R^2 = 0.9983	R^2(adjusted) = 0.9846		

Table 5
Analysis of variance factorial fit: % Rem versus pH, C_o, m, t and central point.

Source	DF	Contribution	Adj. SS	Adj. MS	F-value	*P*-value
Model	16	99.83%	15569.1	973.1	72.78	0.014
Linear	4	81.70%	12742.0	3185.5	238.26	0.004
pH	1	75.83%	11826.6	11826.6	884.59	0.001
C_o	1	4.71%	734.7	734.7	54.95	0.018
m	1	1.01%	157.4	157.4	11.77	0.075
t	1	0.15%	23.3	23.3	1.74	0.318
2-way interaction	6	10.35%	1613.9	269.0	20.12	0.048
pH.Co	1	7.22%	1126.3	1126.3	84.24	0.012
pH.m	1	0.00%	0.3	0.3	0.02	0.894
pH.t	1	1.20%	187.9	187.9	14.05	0.064
C_o.m	1	0.48%	74.6	74.6	5.58	0.142
C_o.t	1	0.85%	133.2	133.2	9.96	0.087
m.t	1	0.59%	91.6	91.6	6.85	0.120
3-way interaction	4	3.49%	545.0	136.2	10.19	0.091
pH.Co.m	1	0.50%	78.3	78.3	5.86	0.137
pH.Co.t	1	0.00%	0.6	0.6	0.04	0.857
pH.m.t	1	1.39%	217.5	217.5	16.27	0.056
C_o.m.t	1	1.59%	248.6	248.6	18.60	0.050
4-way interaction	1	2.65%	413.0	413.0	30.89	0.031
pH.Co.m.t	1	2.65%	413.0	413.0	30.89	0.031
Central point (cp)	1	1.64%	255.1	255.1	19.08	0.049
Error	2	0.17%	26.7	13.4		
Total	18	100.00%				

increase in % Rem, which the user would not perceive during the optimization of batch adsorption using univariate analysis.

In contrast, when using a full factorial design, information about the interactions of factors can be obtained, as observed in this work.

The third most important factor in the optimization of the response (% Rem) was C_o, which had a negative coefficient, meaning that an increase in C_o leads to a decrease in % Rem, as is usually expected for any batch adsorption system [33,34]. The fourth most important factor in the optimization of the response was the interaction of the four factors pH·C_o·m·t, which has a positive coefficient, and the fifth factor was an interaction of three factors (C_o·m·t). The factors m and t only appeared in the overall optimization of % Rem as parts of interaction factors; however, in the response of q, m had a negative coefficient.

Considering that two responses were used in this work to obtain a maximum q and% Rem, the desirability function of the DOE was performed. The desirability function is an optimization method that considers both responses (q and % Rem) to furnish values of variables that would increase both responses. Therefore, the desirability function is an arrangement of values intended to maximize each independent response. Using the desirability function, the optimized conditions were as follows: pH = 2.00; C_o = 40.0 mg L^{-1}; m = 30.0 mg; and t = 3.0 h. The desirability function (D) presents a value of 0.8554, which corresponds to an overall optimization of the two responses by 85.54%.

Conclusions

Magnetized activated carbon nanocomposite (MNSA) was successfully prepared using *Nigella sativa* waste (NSW) and was examined as an adsorbent for Coomassie brilliant blue in aqueous solution under conditions optimized using the design of experiments (DOE). The optimum conditions obtained from the desirability function were as follows: initial pH of adsorption 2.00; initial dye concentration of 40.0 mg/L; adsorbent mass of 30.0 mg; and contact time between the adsorbent and adsorbate of 3.0 h. The results of the present work suggest that agro-industrial wastes could be turned onto valuable, efficient and cost-effective adsorbents for wastewater treatment; furthermore, by applying a full factorial design, information about the interactions of the factors that affect the optimization of a suggested method could be obtained, as observed in this work. To continue this work, adsorption experiments will be performed using the conditions described above and applied to real wastewater samples.

Conflict of interest

The authors have declared no conflict of interest.

Compliance with Ethics Requirements

This article does not contain any studies with human or animal subjects.

Acknowledgements

The authors are grateful to the Faculty of Science at Cairo University, the Agricultural Research Center and the National Council for Scientific and Technological Development (CNPq, Brazil) for their support in accomplishing this work.

References

[1] Abdel-Ghani NT, El-Chaghaby GA, Rawash E-SA, Lima EC. Adsorption of coomassie brilliant blue R-250 dye onto novel activated carbon prepared from *Nigella sativa* L. waste: equilibrium, kinetics and thermodynamics. J Chil Chem Soc 2017;62:3505–11.
[2] Ata S, Imran Din M, Rasool A, Qasim I, Ul Mohsin I. Equilibrium, thermodynamics, and kinetic sorption studies for the removal of coomassie brilliant blue on wheat bran as a low-cost adsorbent. J Anal Methods Chem 2012;2012:1–8.
[3] Sandhya S, Sarayu K, Swaminathan K. Determination of kinetic constants of hybrid textile wastewater treatment system. Bioresour Technol 2008;99:5793–7.
[4] Afkhami A, Saber-Tehrani M, Bagheri H. Modified maghemite nanoparticles as an efficient adsorbent for removing some cationic dyes from aqueous solution. Desalination 2010;263:240–8.
[5] Xu P, Zeng GM, Huang DL, Feng CL, Hu S, Zhao MH, et al. Use of iron oxide nanomaterials in wastewater treatment: a review. Sci Total Environ 2012;424:1–10.

[6] Nethaji S, Sivasamy A, Mandal AB. Preparation and characterization of corn cob activated carbon coated with nano-sized magnetite particles for the removal of Cr(VI). Bioresour Technol 2013;134:94–100.
[7] Zargar B, Parham H, Rezazade M. Fast removal and recovery of methylene blue by activated carbon modified with magnetic iron oxide nanoparticles. J Chinese Chem Soc 2011;58:694–9.
[8] Gupta VK, Agarwal S, Saleh TA. Chromium removal by combining the magnetic properties of iron oxide with adsorption properties of carbon nanotubes. Water Res 2011;45:2207–12.
[9] Saleh TA, Naeemullah Tuzen M, Sarı A. Polyethylenimine modified activated carbon as novel magnetic adsorbent for the removal of uranium from aqueous solution. Chem Eng Res Des 2017;117:218–27.
[10] Saleh TA, Al-Absi AA. Kinetics, isotherms and thermodynamic evaluation of amine functionalized magnetic carbon for methyl red removal from aqueous solutions. J Mol Liq 2017;248:577–85.
[11] Saleh TA, Tuzen M, Sarı A. Magnetic activated carbon loaded with tungsten oxide nanoparticles for aluminum removal from waters. J Environ Chem Eng 2017;5:2853–60.
[12] Tuzen M, Sarı A, Saleh TA. Response surface optimization, kinetic and thermodynamic studies for effective removal of rhodamine B by magnetic AC/CeO2 nanocomposite. J Environ Manage 2018;206:170–7.
[13] Saleh TA, Tuzen M, Sarı A. Polyamide magnetic palygorskite for the simultaneous removal of Hg(II) and methyl mercury; with factorial design analysis. J Environ Manage 2018;211:323–33.
[14] Altıntıg E, Altundag H, Tuzen M, Sarı A, Sarı A. Effective removal of methylene blue from aqueous solutions using magnetic loaded activated carbon as novel adsorbent. Chem Eng Res Des 2017;122:151–63.
[15] Singh KP, Gupta S, Singh AK, Sinha S. Optimizing adsorption of crystal violet dye from water by magnetic nanocomposite using response surface modeling approach. J Hazard Mater 2011;186:1462–73.
[16] Saleh TA. Isotherm, kinetic, and thermodynamic studies on Hg(II) adsorption from aqueous solution by silica- multiwall carbon nanotubes. Environ Sci Pollut Res Int 2015;22:16721–31.
[17] Saleh TA. Nanocomposite of carbon nanotubes/silica nanoparticles and their use for adsorption of Pb(II): from surface properties to sorption mechanism. Desalin Water Treat 2016;57:10730–44.
[18] Lingamdinne LP, Koduru JR, Chang Y-Y, Karri RR. Process optimization and adsorption modeling of Pb(II) on nickel ferrite-reduced graphene oxide nanocomposite. J Mol Liq 2018;250:202–11.
[19] Gupta VK, Nayak A. Cadmium removal and recovery from aqueous solutions by novel adsorbents prepared from orange peel and Fe_2O_3 nanoparticles. Chem Eng J 2012;180:81–90.
[20] dos Reis GS, Wilhelm M, de Almeida Silva TC, Rezwan K, Sampaio CH, Lima EC, et al. The use of design of experiments for the evaluation of the production of surface rich activated carbon from sewage sludge via microwave and conventional pyrolysis. Appl Therm Eng 2016;93:590–7.
[21] Leite AB, Saucier C, Lima EC, dos Reis GS, Umpierres CS, Mello BL, et al. Activated carbons from avocado seed: optimisation and application for removal of several emerging organic compounds. Environ Sci Pollut Res 2017.
[22] Chen B, Chen Z, Lv S. A novel magnetic biochar efficiently sorbs organic pollutants and phosphate. Bioresour Technol 2011;102:716–23.
[23] Hao Z, Wang C, Yan Z, Jiang H, Xu H. Magnetic particles modification of coconut shell-derived activated carbon and biochar for effective removal of phenol from water. Chemosphere 2018;211:962–9.
[24] Atkinson JD, Fortunato ME, Dastgheib SA, Rostam-Abadi M, Rood MJ, Suslick KS. Synthesis and characterization of iron-impregnated porous carbon spheres prepared by ultrasonic spray pyrolysis. Carbon NY 2011;49:587–98.
[25] Han S, Zhao F, Sun J, Wang B, Wei R, Yan S. Removal modified of p-nitrophenol from aqueous activated carbon solution by magnetically. J Magn Magn Mater 2013;341:133–7.
[26] Ghaedi M, Hajjati S, Mahmudi Z, Tyagi I, Agarwal S, Maity A, et al. Modeling of competitive ultrasonic assisted removal of the dyes - Methylene blue and Safranin-O using Fe_3O_4 nanoparticles. Chem Eng J 2015;268:28–37.
[27] Mohan D, Sarswat A, Singh VK, Alexandre-Franco M, Pittman CU. Development of magnetic activated carbon from almond shells for trinitrophenol removal from water. Chem Eng J 2011;172:1111–25.
[28] Montogomery DC. Design and analysis of engineering experiments. 5th ed. John Wiley & Sons; 2001.
[29] Abdel-Ghani NT, Hegazy AK, El-Chaghaby GA, Lima EC. Factorial experimental design for biosorption of iron and zinc using *Typha domingensis* phytomass. Desalination 2009;249:343–7.
[30] Lima EC, Royer B, Vaghetti JCP, Brasil JL, Simon NM, dos Santos AA, et al. Adsorption of Cu(II) on *Araucaria angustifolia* wastes: determination of the optimal conditions by statistic design of experiments. J Hazard Mater 2007;140:211–20.
[31] Brasil JL, Ev RR, Milcharek CD, Martins LC, Pavan FA, dos Santos AA, et al. Statistical design of experiments as a tool for optimizing the batch conditions to Cr(VI) biosorption on *Araucaria angustifolia* wastes. J Hazard Mater 2006;133:143–53.
[32] Royer B, Lima EC, Cardoso NF, Calvete T, Bruns RE. Statistical design of experiments for optimization of batch adsorption conditions for removal of reactive red 194 textile dye from aqueous effluents. Chem Eng Commun 2010;197:775–90.
[33] da Silva LG, Ruggiero R, Gontijo PD, Pinto RB, Royer B, Lima EC, et al. Adsorption of Brilliant Red 2BE dye from water solutions by a chemically modified sugarcane bagasse lignin. Chem Eng J 2011;168:620–8.
[34] Alencar WS, Lima EC, Royer B, dos Santos BD, Calvete T, da Silva EA, et al. Application of aqai stalks as biosorbents for the removal of the dye procion blue MX-R from aqueous solution. Sep Sci Technol 2012;47:513–26.